13TH CANADIAN MASONRY SYMPOSIUM
HALIFAX, CANADA
JUNE 4TH – JUNE 7TH 2017

QUANTIFICATION OF NON-STRUCTURAL DAMAGE IN UNREINFORCED MASONRY WALLS INDUCED BY GEOTHERMAL RESERVOIR EXPLORATION USING QUASI-STATIC CYCLIC TESTS

Didier, Max[1]; Abbiati, Giuseppe[1]; Broccardo, Marco[1]; Beyer, Katrin[2]; Danciu, Laurentiu[3]; Petrović, Miloš[1]; Mojsilović, Nebojša[1] and Stojadinović, Božidar[1]

ABSTRACT

In Basel and St. Gallen, Switzerland, two pilot enhanced geothermal systems projects caused two sequences of induced earthquakes with magnitude up to 3.5. In Basel, hairline cracks in walls and non-structural damage arose from the largest of the events. This led to damage claims of approximately 7-10 million of Swiss Francs. It follows that prediction and quantification of non-structural damage due to induced ground motions is central for estimating related financial risk. This perspective motivated the authors to develop a procedure for quantifying plaster cracks on URM walls caused by induced ground motions. Test protocols consisting of horizontal displacement sequences were produced for a reference masonry building considering a pool of ground motions consistent with the induced seismic hazard and using the rainflow counting algorithm. A quasi-static cyclic test campaign was conducted on five URM walls. An automatic procedure based on digital imaging correlation and image processing was developed to quantify plaster damage. The entire testing campaign as well as preliminary analyses are presented in this paper.

KEYWORDS: *geothermal reservoir explorations, induced seismicity, unreinforced masonry walls, quasi-static testing, crack analysis, digital image correlation, image processing.*

INTRODUCTION

New sources of energy as well as new schemes for storing waste water and carbon-dioxide are relying on hydro-fracking and hydro-shearing. Both are methods to increase the permeability of rock by injecting high-pressure water. In the case of hydro-fracking, the high-pressure water causes new fractures in the rock, while in the hydro-shearing case the pressure increment causes slips in

[1]Institute of Structural Engineering (IBK), Swiss Federal Institute of Technology (ETH) Zurich, didierm@ethz.ch
[2]Earthquake Engineering and Structural Dynamics Laboratory (EESD), Swiss Federal Institute of Technology (EPF) Lausanne
[3]Swiss Seismological Service (SED), Swiss Federal Institute of Technology (ETH) Zurich

existing faults. However, these technologies also have drawbacks. Hydro-fracking and hydro-shearing create long sequences of low-magnitude-induced earthquakes (usually, the moment magnitudes are below 3) and can potentially trigger larger magnitude events. In Switzerland, these technologies have been used in two pilot deep geothermal energy projects in Basel (2006, 2007) and St. Gallen (2013) [1]. Both projects induced earthquakes, up to a moment magnitude of 3.4 in Basel and a moment magnitude of 3.5 in St. Gallen. In Basel, even if damage was limited to cosmetic cracks (e.g. hairline cracks in walls of nearby masonry buildings), the resulting damage claims were estimated to approximately 7-10 million of Swiss Francs. Therefore, prediction and quantification of potential non-structural damage due to induced ground motions is important for estimating both, the financial risk and insurance policies.

The main goal of this study is, thus, to understand the damaging potential of repeated induced and triggered earthquake motions for typical Swiss unreinforced masonry (URM) construction. URM walls are widely used in Switzerland, in historical buildings as well as in contemporary buildings. To investigate plaster cracking on URM walls caused by induced ground motions, a quasi-static cyclic test campaign was recently conducted at the Swiss Federal Institute of Technology (ETH) Zurich. Firstly, a pool of relevant induced and natural ground motions was selected to calculate the response of an elastic single-degree-of-freedom system, which represents a reference masonry building. Quasi-static cyclic displacement-controlled test sequences were then produced by applying the rainflow counting algorithm to each displacement response history. Plastered URM wall specimens were then tested in a three-actuator-setup under constant gravity load by applying the horizontal displacement test sequences. During the test, in-plane displacement and deformation fields of the plastered surface were measured using Digital Imaging Correlation (DIC). Image Processing (IP) was then employed to quantify the fraction of cracked surface. This paper provides an overview of the testing campaign and discusses preliminary results.

SELECTION OF REPRESENTATIVE INDUCED SEISMICITY RECORDS

In order to derive test protocols representative of the Swiss induced seismic hazard, 28 records have been collected and grouped into two bins defined using moment magnitude M and hypocenter distance R_{hypo} as follows: BIN 1: $M \in [3.0, 3.8]$ & $R_{hypo} \in$ [0, 15] km, and BIN 2: $M \in (3.8, 5]$ & $R_{hypo} \in$ [0, 20] km. The dataset of induced motions for BIN 1 and BIN 2 is built on: the PEER NGA-east database [2]; the Basel 2007 and St. Gallen 2013 records aroused from the induced seismicity sequences; and a selection of West US induced motions. Since the number of records was insufficient for deriving a robust load sequence, an augmented data set has been designed. The augmented dataset has been defined by increasing the number of records. BIN 1 was augmented by scaling the given records. The scaling procedure was based on magnitude and derived as follows:

i. A set of ground motion predictive equations (GMPEs) developed for induced seismicity was selected. In this study, the GMPEs set was based on Atkinson [3] and Douglas [4];
ii. The GMPE reference median value for the recorded M and given R_{hypo} was computed;
iii. Five new magnitude levels were defined: 3.0, 3.2, 3.4, 3.6 and 3.8;

iv. The GMPE median was recomputed for new magnitude levels and same distances;
v. The scaling factor was derived as the ratio between median GMPE computed as in point iv. and the reference GMPE median as computed in point ii.;
vi. The scaling factor was applied to the recorded time series with original M and R_{hypo}; this resulted in a total number of 70 records.

BIN2 was augmented with 63 European natural records with the same magnitude, distance and soil conditions. The records belong to soil classes A and B (according to Eurocode 8). The total number of motions of the augmented BIN 2 was 72. Figure 1 shows the augmented dataset.

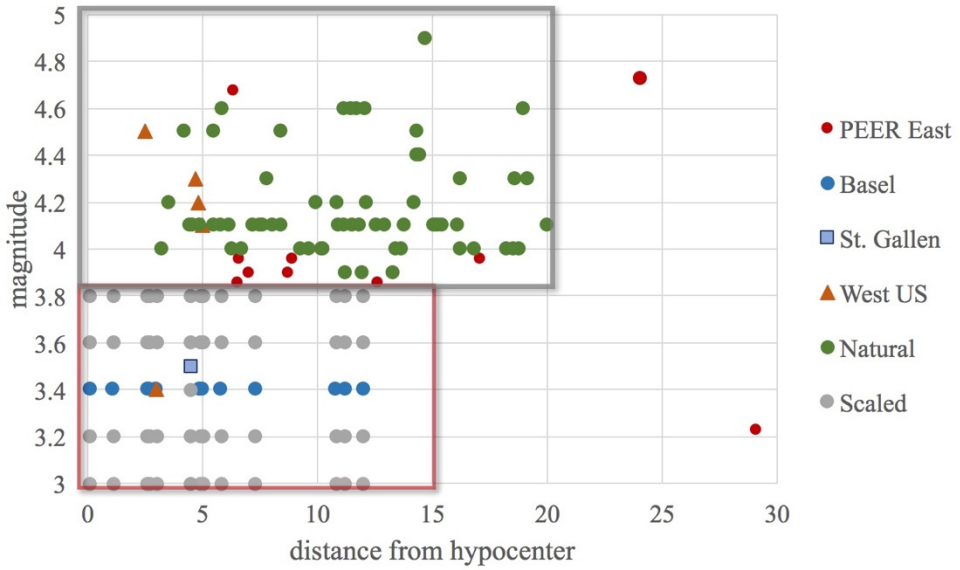

Figure 1: Augmented database used to compute the load sequences (BIN 1: red box; BIN 2: grey box)

DERIVATION OF THE TEST PROTOCOLS

Test protocols representative of induced seismicity consist on alternating displacement sequences with monotonically increasing magnitude and were derived considering the reference masonry 1-story building depicted in Figure 2, which is modeled as a linear elastic single-degree-of-freedom (S-DOF) system with period $T = 0.3\ s$ and damping ratio $\zeta = 2\ \%$.

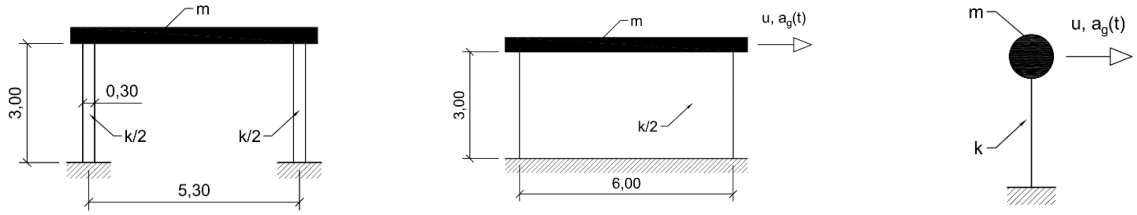

a) **b)** **c)**

Figure 2: Reference masonry building for the calculation of seismic responses: a) front view; b) side view; c) equivalent S-DOF system

The displacement response history of the equivalent S-DOF system was calculated for each ground motion of the dataset using the Newmark method with $\gamma = 0.5$ and $\beta = 0.25$ [5] and time integration step $0.005\ s$. The equation of motion reads,

$$m\ddot{u} + c\dot{u} + ku = -ma_g(t) \quad (1)$$

where $m = 4.37e7\ kg$, $c = 3.66e7\ Ns/m$ and $k = 1.92e10\ N/m$ are mass, damping and stiffness parameters, respectively, whilst u and a_g are displacement response and seismic accelerogram. According to the procedure shown in Mergos and Beyer [6], the rainflow counting algorithm [7] was used to extract 50 bins from any single displacement response history, each characterized by mean offset, amplitude and number of an equivalent set of constant cycles. Information concerning mean offsets, always rather small compared to corresponding amplitudes, was neglected as well as number of cycles. Then, for each response history, bin amplitudes were sorted in descending order and an empirical cumulate distribution was calculated for each bin over the entire response history set. The 99 % quantile of such empirical cumulate distribution is referred to as rough test protocol. In order to ensure a loading sequence with an increasing displacement amplitude, a smooth test protocol was derived by surrogating the rough displacement sequence with the exponential function suggested by Mergos and Beyer [6], which reads,

$$\Delta_k = b + a \cdot e^{\left(\left(\frac{k-1}{N-1}\right)^{\alpha} - 1\right)} \quad (2)$$

where a, b and α are coefficients, k is the cycle index ranging from 1 to N, that is, the total number of cycles of the loading sequence. In order to avoid loading cycles too small to have some effect on the structure, a minimum amplitude $\Delta_{min} = 0.1\ mm$ was set, while the maximum amplitude $\Delta_{max} = 9.5\ mm$ was obtained from the rough protocol. The parameter α minimizes the norm of the square error between the rough and the smooth test protocols. Figure 3 a) reports the output of the rainflow count: grey lines represent bin amplitudes corresponding to single displacement response histories, while the dashed black line represents the 99% quantile of the amplitude empirical cumulate distribution, which was used to derive a rough protocol for the ground motion dataset BIN2_99. Figure 3 b) compares rough and smooth protocols for the same ground motion dataset. The test protocol was obtained by concatenating a sequence of triangular displacement cycles of increasing amplitudes, which were uniformly interpolated from the smooth protocol. In the particular case of the BIN2_99 protocol, it was decided to consider 29 amplitude values. A length scaling factor of 1.2/3.0 (the ratio of the height of the specimen to the height of the masonry wall prototype, Figure 2) was applied to the test protocol in order to scale the drift values correctly. In addition, the test protocol proposed by Beyer and Mergos [8], referred to as NAMC hereinafter, was used to perform quasi-static cyclic tests. Table 1 summarizes the test protocols used in this test campaign. Figure 4 shows test protocols BIN2_99 and NAMC. A constant actuator velocity of 2 mm/min was considered for the BIN2_99 protocol, while the actuator velocity ranged from 1 to 4 mm/min for the NAMC protocol.

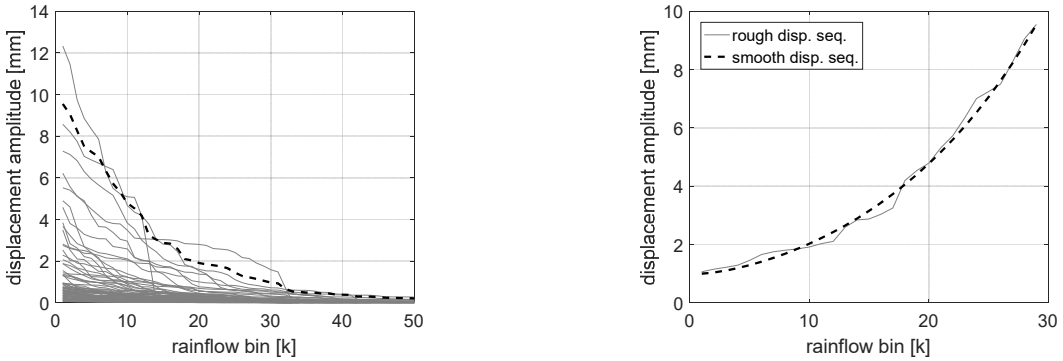

a) **b)**

Figure 3: a) Derivation of the rough protocol for the ground motion dataset BIN 2; b) Rough and smooth protocol for the ground motion dataset BIN 2

Table 1: Test protocols

Test protocol name	Ground motion dataset	Amplitude quantile
BIN1_975	BIN 1 (Figure 1)	97.5%
BIN2_99	BIN 2 (Figure 1)	99%
NAMC	Beyer and Mergos (2014)	97.5%

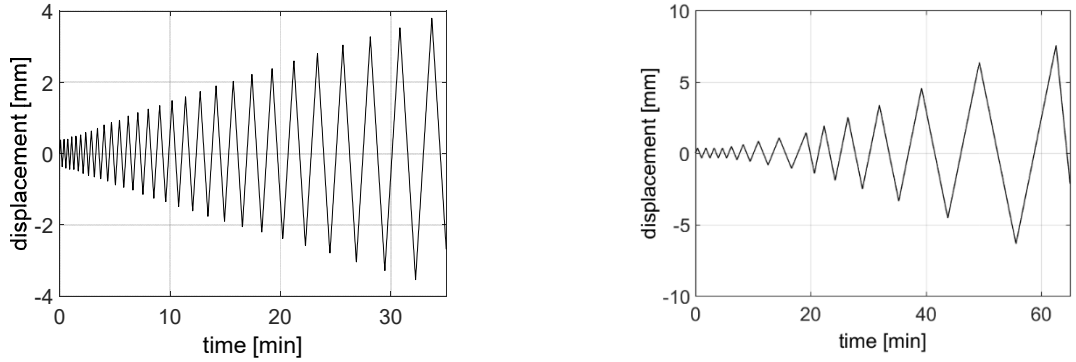

a) **b)**

Figure 4: Test protocols: a) BIN2_99; b) NAMC

DESCRIPTION OF THE EXPERIMENTAL CAMPAIGN

Unreinforced masonry wall specimens

Five $1.20\ x\ 1.20\ x\ 0.15\ m$ URM wall specimens were built and tested in the Structural Testing Laboratory at ETH Zurich. Convectional hollow Swiss clay bricks (produced by *ZZ Wancor AG*, corresponding to *Swissbrick B15/19*) were used to manufacture each wall. The mortar used for the joints was *Weber mur 920* (*Zementmörtel M15*). The average vertical compression strength of walls, f_c = 4.50 MPa, was determined 5 months after the construction of the specimens [9]. The front side of each wall was plastered at least 28 days before testing with a 12-14 mm thick plaster

layer (*Zement-Kalk 29* produced by *Granol*). No plaster was applied to the back side. Figure 5 shows the tested URM wall.

a) **b)**

Figure 5: URM wall specimen: a) without plaster; b) with plaster

As shown in Figure 5, each wall was placed on a concrete foundation, which was then fixed to the reaction floor by post-tensioning bars. A mortar layer connected the wall top to the loading frame of the experimental setup, which is described in the following subsection. The same mortar as used for the joints of the wall was used to produce 10mm thick and fully filled bed and head joints. In order to avoid vertical loads on plaster, the top mortar layer was only applied on the bricks, leaving the plaster free. Note that due to the variable height of the top mortar layer, a small angle has been observed between the top of the wall and the movement of the horizontal actuator. In the following, this angle is considered as negligible.

Test setup

The test setup is a steel loading frame and three servo-hydraulic actuators of 250 kN capacity each. A horizontal actuator, used in displacement control mode, imposed the horizontal displacement test protocol sequence to the wall through a steel loading beam. A laser distance sensor was used to measure the feedback displacement at the top level of the specimen. Two vertical actuators imposed the gravity load to the wall in force control mode. The rotation of the loading beam was not controlled: instead, the vertical actuator forces were controlled in conjunction with the horizontal actuator to impose no moment at the top of the specimen. Thus, the specimen was tested with cantilever boundary conditions.

Seven external Linear Variable Differential Transformers (LVDT) measured local displacements at the bottom and the top level of the wall, as well as foundation slip. Figure 6 reports a schematic of the test setup with labels of actuators and sensors while Table 2 reports a short description of external LVDT sensors.

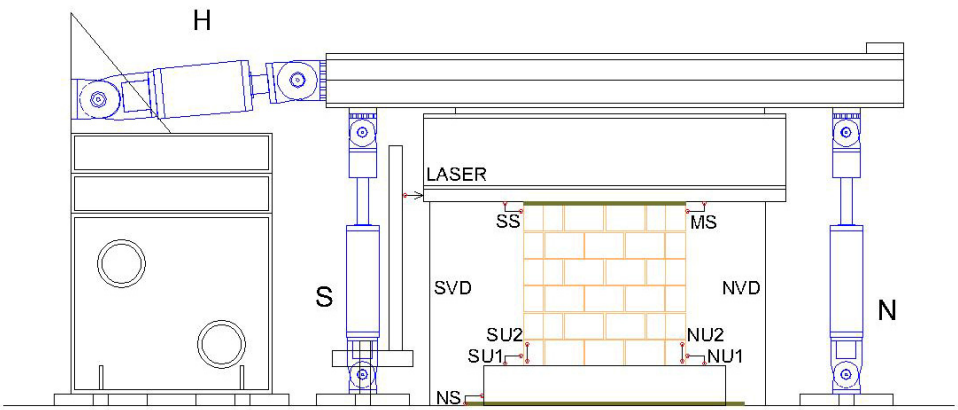

Figure 6: Experimental setup

Table 2: External sensors used during the test campaign

Label	Measured quantity
MS	Drift between beam and wall, North
SS	Drift between beam and wall, South
SU1	Drift between concrete foundation and wall, South
SU2	Uplift of the wall from concrete foundation, South
NU1	Drift between concrete foundation and wall, North
NU2	Uplift of the wall from concrete foundation, North
NS	Drift between concrete foundation and floor, South
SVD	Vertical displacement of beam relative to floor, South
NVD	Vertical displacement of beam relative to floor, North

Digital Image Correlation (DIC) was used to acquire in-plane displacement and strain fields on the plaster surface during the tests. Figure 7 provides an overview of the DIC setup including the speckling pattern.

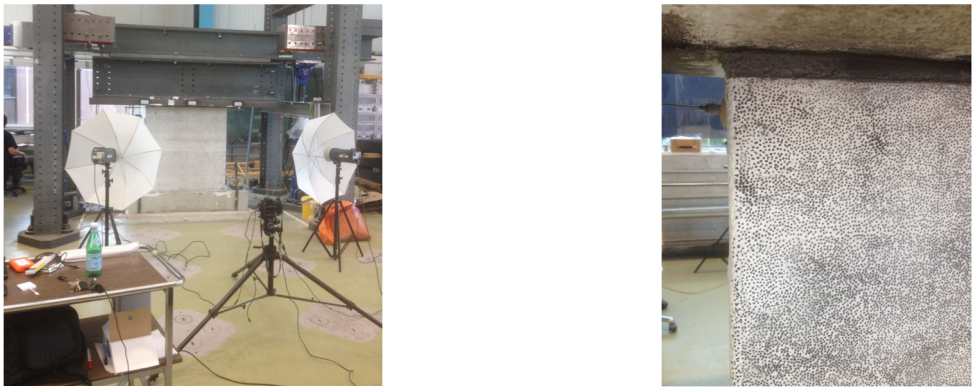

a) **b)**

Figure 7: DIC setup: a) camera and flashlight positions; b) detail of the random speckle pattern applied to the plaster surface

A black and white random speckle pattern was painted on the plastered surface of the specimen. The dot size of about $1 \div 1.5\ mm$ was calibrated to obtain $3 \div 4$ pixel size dots in digital images, which was proved to be an optimal setting for the target measurements [10]. Digital images were taken with a NIKON D810 digital camera with a 50mm lens, while two flashlights guaranteed a uniform illumination and optimal balance of the plaster images. Picture shooting was triggered from the actuator controller at pre-defined displacement values of the test protocol.

Test program

A vertical load equal to $96.30\ kN$ (including the weight horizontal steel beams), i.e. 10% of the vertical compressive strength, was applied to the specimen using a linear ramp before starting the displacement test protocol. Table 3 summarizes the test program. Note that the specimens were tested using two or more test protocols.

Table 3: Summary of the test program

Test ID	Wall ID	Test protocol	Date
1	0	NAMC	2016/07/11
2	1	BIN1_975	2016/07/27
3	1	BIN1_975	2016/07/29
4	1	BIN2_99	2016/08/08
5	1	NAMC	2016/08/08
6	2	BIN2_975	2016/08/11
7	2	NAMC	2016/08/11
8	3	BIN2_99	2016/08/16
9	3	NAMC	2016/08/16
10	4	BIN2_99	2016/08/18
11	4	NAMC	2016/08/18

EXPERIMENTAL RESULTS

Since test protocol BIN1_975 was not producing observable damage to the walls, the following discussions focus on results related to test protocols BIN2_99 and NAMC. Figure 8 compares the horizontal force-displacement response measured on Test #6 (Wall #2, BIN2_99 test protocol) and Test #5 (Wall #1, NAMC test protocol).

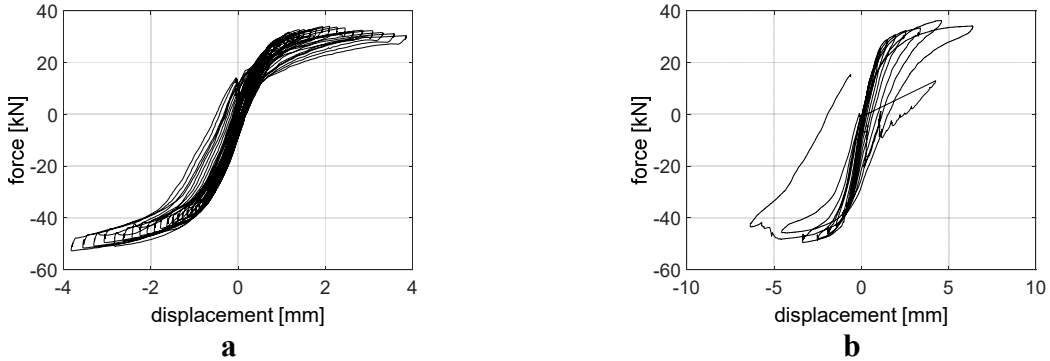

Figure 8: Horizontal force-displacement response measured on: a) Test #6 (Wall #2, BIN2_99 test protocol); b) Test #5 (Wall #1, NAMC test protocol)

The rocking response of the wall is evident in Figure 8 a). This behavior is ascribed to the adopted cantilever configuration, which allowed walls to uplift starting at small displacement amplitudes and rotate as rigid bodies. As a result, the plaster was preserved from cracking up to 2 mm displacement amplitude. On the other hand, the response developed to the NAMC test sequence, shown in Figure 8 b), is more irregular and the corresponding damage pattern includes heavy cracks in the plaster and the bricks. The asymmetric restoring force plateau was shown to be sensitive to the initial loading direction. For all tests considered in this paper, the first displacement ramp was applied from South to North.

DIC processing of raw pictures was conducted with the Vid2D software [11], which provided displacement and von Mises strain maps of the speckled area of the wall. It is important to emphasize that DIC provides a very large amount of data to be post-processed. In order to post-process damage information avoiding human supervision, an automatic Image Processing (IP) procedure was developed. It is summarized in the following steps:

1. Von Mises strain maps computed with Vic2D were imported into Matlab as matrices;
2. Von Mises strain maps were then converted to grayscale pictures considering a strain interval ranging between 0 and 0.1. These values were calibrated to maximize the signal-to-noise ratio of grayscale pictures over different test protocols;
3. Grayscale von Mises strain maps were converted to black-and-white using an average optimal threshold value for black-to-white transition equal to 0.15 estimated using the *graythresh* function of the Image Processing Toolbox of Matlab [12];
4. For all binary (black-and-white) von Mises strain maps of index k varying from 1 to N, where N is the number of pictures, a cumulate binary von Mises strain map was calculated as the result of a logic OR operation between all binary von Mises strain maps from 1 to k;
5. A damage score was calculated as the percentage of white pixels on cumulate binary von Mises strain maps, which allows for quantify the amount of damage affecting the plaster surface.

Figure 9 shows an overview of the IP procedure for test sequences NAMC (Wall #1) and BIN2_99 (Wall #2). All pictures refer to the last load step of the corresponding protocol.

As shown in Figure 9, the cumulate binary von Mises strain map qualitatively shows a very good correlation with the damage level observed in raw pictures. In fact, an extremely slight crack pattern, almost invisible to the bare eyes, corresponds to Test #6 (Wall #2, BIN2_99 test protocol), where the cumulate binary von Mises strain map highlights a small damaged area. On the other hand, a heavy crack pattern is observed on Test #5 (Wall #1, NAMC test protocol), where the cumulate binary maps indicate a larger extent of damage. Finally, Figure 10 compares histories of the damage scores calculated for the same two tests. It is important to stress that the introduced damage score does not represent the actual cracked surface but it is a measure proportional to the damaged area. Further work needs to be done to provide a robust correlation between the qualitative damage observed on raw images, which could also easily be taken during on-site surveys, and the quantitative damage score introduced in this paper.

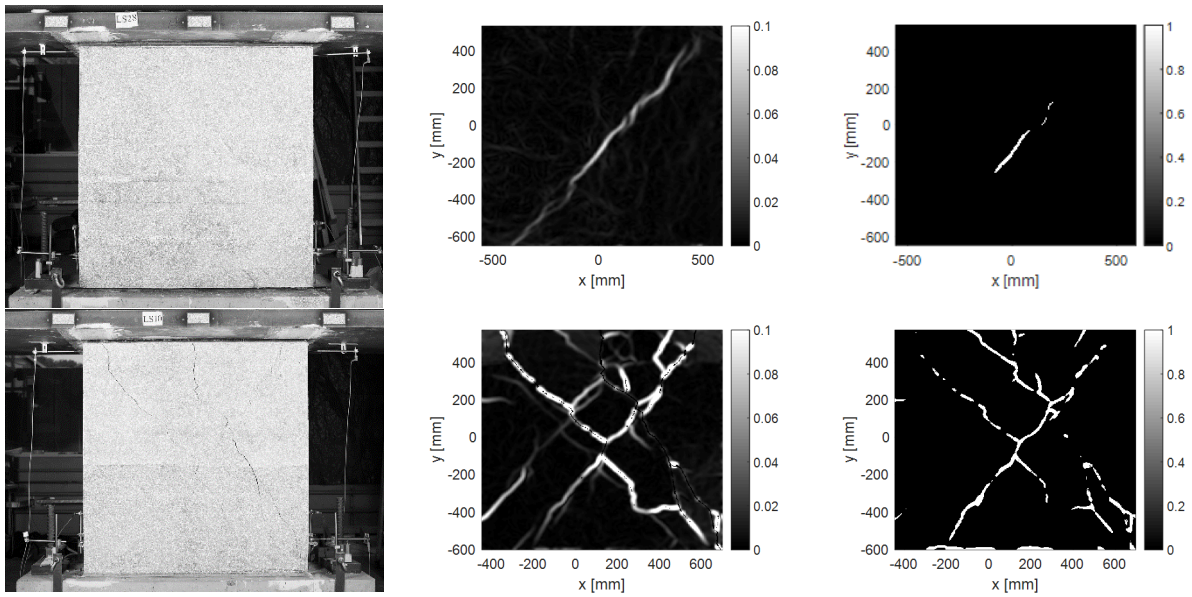

a) **b)** **c)**

Figure 9: Overview of the DIC/IP procedure: a) raw picture; b) grayscale von Mises strain map; c) cumulate binary von Mises strain map. Upper row refers to Test #6 (Wall #2, BIN2_99 test protocol) while lower row refers to Test #5 (Wall #1, NAMC test protocol)

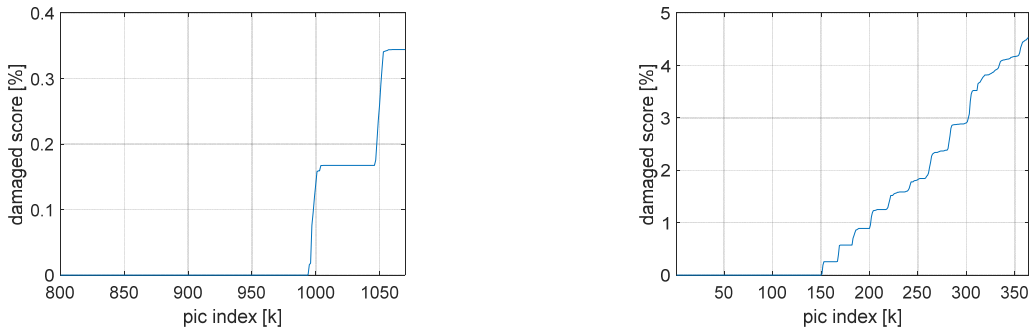

a) **b)**

Figure 10: Damage score histories of: a) Test #6 (Wall #2, BIN2_99 test protocol); b) Test #5 (Wall #1, NAMC test protocol)

CONCLUSION

In order to investigate the plaster cracks on URM walls caused by induced ground motions, a comprehensive quasi-static cyclic test campaign was recently conducted at the ETH Zurich. Test protocols for quasi-static cyclic displacement-controlled tests, representative of induced ground motion were produced for a reference masonry building considering a pool of ground motions consistent with the induced seismic hazard and applying the rainflow-counting algorithm. Five walls were tested in a cantilever configuration using the test protocols and an automatic procedure based on digital imaging correlation and image processing was developed to quantify plaster damage. The preliminary analysis shown in this paper is confined to a pair of tests but further work is needed to perform a statistical elaboration of the entire data.

ACKNOWLEDGEMENTS

The authors wish to acknowledge the help of the technicians of the ETH Zurich Structural Testing Laboratory, Mr. Dominik Werne and Mr. Pius Herzog. The authors gratefully acknowledge the funding from the Swiss Competence Center for Energy Research (SCCER): Supply of Electricity (SoE), and ETH Zurich and EPF Lausanne. The findings and conclusions presented in this paper are those of the authors and do not necessarily represent the views of the sponsors.

REFERENCES

[1] Mignan, A., Landtwing, D., Kästli, P., Mena, B., & Wiemer, S. (2015). "*Induced seismicity risk analysis of the 2006 Basel, Switzerland, Enhanced Geothermal System project: Influence of uncertainties on risk mitigation*", Geothermics, 53, 133–146.

[2] Ngawest2.berkeley.edu. (2017). PEER Ground Motion Database - PEER Center. [online] Available at: http://ngawest2.berkeley.edu/ [Accessed 29 Jan. 2017].

[3] Atkinson, Gail M. "Ground-motion prediction equation for small-to-moderate events at short hypocentral distances, with application to induced-seismicity hazards." *Bulletin of the Seismological Society of America* (2015).

[4] Douglas, John, Benjamin Edwards, Vincenzo Convertito, Nitin Sharma, Anna Tramelli, Dirk Kraaijpoel, Banu Mena Cabrera, Nils Maercklin, and Claudia Troise. "Predicting ground motion from induced earthquakes in geothermal areas." *Bulletin of the Seismological Society of America* 103, no. 3 (2013): 1875-1897.

[5] Newmark, Nathan M. "A Method of Computation for Structural Dynamics. "*Journal of the Engineering Mechanics Division*, ASCE, (1959)

[6] Mergos, P. E., Beyer, K. (2014). "Loading protocols for European regions of low to moderate seismicity." *Bulletin of earthquake engineering*, 12(6), 2507-2530.

[7] Downing, S.D. and Socie, D.F., (1982). "Simple rainflow counting algorithms." *International Journal of Fatigue*, 4(1), 31-40.

[8] Beyer, K., Mergos, P., (2015). "Sensitivity of drift capacities of URM walls to cumulative damage demands and implications on loading protocols for quasi-static cyclic tests." *Proc., 12th North American Masonry Conference Masonry*, Denver, Colorado, on USB.

[9] Bitterli, S., (2014). "Technischer Bericht Versuche an Mauerwerkselementen mit geneigten Lagerfugen", ETH Zürich, Masterarbeit.

[10] Mojsilović, N and Salmanpour, A. H., (2016). "Masonry walls subjected to in-plane cyclic loading: application of digital image correlation for deformation field measurement", *International Journal of Masonry Research and Innovation*, 1(2).

[11] Correlatedsolutions.com, (2017). "Correlated Solutions – VIC-2D™", [online] Available at: http://correlatedsolutions.com/vic-2d/ [Accessed 26 Jan. 2017].

[12] MATLAB Release 2015b (2015): *The MathWorks, Inc*., Natick, Massachusetts, United States.